International Journal of Heat and Mass Transfer 52 (2009) 4553–4563

Contents lists available at ScienceDirect

International Journal of Heat and Mass Transfer

journal homepage: www.elsevier.com/locate/ijhmt

Generalized correlations for predicting heat transfer and pressure drop in plate heat exchanger channels of arbitrary geometry

D. Dović [a,*], B. Palm [b], S. Švaić [a]

[a] Department of Thermal and Process Engineering, University of Zagreb, 10 000 Zagreb, Croatia
[b] Department of Energy Technology, Royal Institute of Technology, S-100 44 Stockholm, Sweden

ARTICLE INFO

Article history:
Received 21 November 2008
Accepted 11 March 2009
Available online 30 May 2009

Keywords:
Chevron plate heat exchangers
Heat transfer
Pressure drop
Basic cell
Semi-analytical correlation
Experimental data

ABSTRACT

Characteristics of the flow in chevron plate heat exchangers are investigated through visualization tests of channels with $\beta = 28°$ and $\beta = 61°$. Mathematical model is then developed with the aim of deriving correlations for prediction of f and Nu for flow in channels of arbitrary geometry (β and b/l). Thermal and hydraulic characteristics are evaluated using analytical solutions for the entrance and fully developed regions of a sinusoidal duct adapted to the basic single cell. The derived correlations are finally adjusted so as to agree with experimental results from tests on channels with $\beta = 28°$ and $\beta = 65°$. f and Nu calculated by the presented correlations are shown to be consistent with experimental data from the literature at Re = 2–10,000, $\beta = (15–67)°$ and b/l = 0.26–0.4.

1. Introduction

The use of plate heat exchangers (PHEs) has increased considerably in the past two decades, and they are now accepted as standard heat transfer equipment in a broad range of heating and cooling applications, operating both in single and two-phase flow regimes. PHEs are characterised by low volume/surface ratio (compactness), high overall heat transfer coefficients and low production and operational costs compared to conventional shell & tube heat exchangers. In spite of their long history of commercial use (since 1960s) there is still a lack of reliable data and generalized solutions available in the literature for calculation of heat transfer and pressure drop. At the same time, published results from thermal and hydraulic tests [1–12] show large mutual discrepancies even when comparing specific chevron angles β, recognized as the most influencing geometric parameter. This calls for further investigation of the basic flow phenomena in PHE channels and analysis of other influencing parameters. Such investigations should also scrutinize the definitions of quantities used in correlations and when presenting experimental results such as the hydraulic diameter, effective flow length and velocity. Alternative definitions may better reflect effects of geometric parameters of the plates, flow regimes and fluid properties on performance.

Several investigations have already been conducted with the aim of exploring the rather complex flow mechanism occurring in chevron channels [13–17]. These investigations have resulted in detection of two flow patterns occurring in single phase flow – the furrow and the longitudinal flow pattern, prevailing in channels with $\beta < 45°$ and $\beta > 60°$, respectively. Studies of Muley et al. [4] and Gaiser and Kottke [14,15] identified the importance of other geometric parameters such as the corrugation depth l and width b on the heat transfer and pressure drop. Only few investigators (Muley et al. [4,5], Wanniarachchi et al. [18]), correlated published experimental thermal–hydraulic data to develop generalized correlations for prediction of heat transfer and pressure drop with the chevron angle β as a variable geometric parameter while Muley et al. [4] also included in their correlation the ratio of developed to projected surface area (which is a function of b/l).

Exploiting the information available from the experimental studies on the basic flow phenomena as well as the thermal hydraulic test data from the literature, Martin [19] developed expressions for calculation of heat transfer and pressure drop which take into account all geometric parameters, which were identified in the previously mentioned articles to have some influence on the flow – the chevron angle β, pressing depth b and the corrugation wave length l.

Influence of the flow distribution inlet and outlet sections design on PHE performance was not separately investigated by any of mentioned authors, although the differences in sections design were identified in some works [4,5] as a possible additional cause of disagreement between published thermal test data. Haseler et al. [16] suggested that these sections can be modelled as the

* Corresponding author.
E-mail address: ddovic@fsb.hr (D. Dović).

0017-9310/$ - see front matter © 2009 Elsevier Ltd. All rights reserved.
doi:10.1016/j.ijheatmasstransfer.2009.03.074

Nomenclature

A_c	channel cross-sectional free flow area, m^2
b	corrugation depth (2 × amplitude of a sine duct), m
D_h	hydraulic diameter, $2b/\varphi$, m
f	Fanning friction factor
f_{app}	apparent Fanning friction factor
$K(\infty)$	incremental pressure drop number
$K_d(\infty)$	momentum flux correction factor
$K_e(\infty)$	kinetic energy correction factor
L	characteristic length, m
L_h	hydrodynamic entrance length, m
L_t	thermal entrance length, m
l	corrugation wave length, m
$\dot{m}$	mass flow rate, kg/s
Nu	Nusselt number, $\alpha D_h/\lambda$
p	corrugation pitch, m
Pr	Prandtl number
Δp	pressure drop, Pa
Re	Reynolds number, $uD_h\rho/\mu$
u	mean velocity, m/s
u_{sine}	velocity of the substream in the furrow, m/s
W	plate width, m
x	axial distance, m
x^+	dimensionless axial distance

Greek symbols

α	heat transfer coeff. referred to developed surface area,W/(m^2 K)
β	corrugation inclination angle relative to vertical direction, °
ϕ	enhancement factor (ratio developed/projected heat transfer surface area)
λ	thermal conductivity, W/(mK)
μ	dynamic viscosity, Ns/m^2
ρ	density, kg/m^3

Subscripts

app	apparent
cell	whole cell
ch	corrug. channel
fully	fully developed
furr	furrow
h	hydraulic
long	longitudinal
sine	sinusoidal duct
w	wall

additional chevron part area (equal to the projected area of the sections), assuming that any poorer heat transfer there can be compensated for by the increased mass flux relative to the chevron region. No information has been found in the literature on the pressure drop in the flow distribution sections. Contribution of the pressure drop in inlet/outlet ports and manifolds is estimated in Shah [20] as normally <10% of the overall pressure drop, depending on a port/manifold size, number of passes and Re number. Shah and Focke [20] also proposed the expressions for predicting pressure drop in ports and manifolds which Muley et al. [4,5] employed to reduce measured overall to the pressure drop in the single channel only, unlike the other mentioned authors who provided no detailed information on the method of determining their pressure drop data.

The research presented in this work represents an effort to contribute to the sparse amount of generalized correlations for prediction of thermal–hydraulic performances of PHEs, as well as to a better understanding of the mechanisms determining heat transfer and pressure drop in chevron channels and the corresponding influence of the flow conditions and geometrical parameters. Accordingly, based on the observations from the presented visualization tests (more details in [21]), here is described a physically based mathematical model for prediction of heat transfer and pressure drop in laminar, transient and turbulent single phase flow in between corrugated plates, valid for plates with chevron angles $\beta = (15–65)°$ and aspect ratios $b/l = (0.26–0.4)$. The model focuses on the single cell, the smallest repeating unit of the channel (Fig. 1) composed of two crossing ducts with (close to) sinusoidal cross sections. The analytical solutions for heat transfer and pressure drop in a channel of sinusoidal geometry are applied to these ducts. Values of f and Nu obtained from the generalized correlations derived within the mathematical model are compared with experimental data recorded in tests on PHEs with $\beta = 28°$ and $\beta = 65°$ and, additionally, with published experimental data and values computed from generalized expressions available in the literature.

2. Characteristics of flow

PHEs consist of a number of narrow channels (av. $D_h \sim 3–4$ mm) each composed by two corrugated plates (Fig. 1) with chevrons inclined by the angle β to the main flow direction between an inlet and an outlet port of the exchanger. Small hydraulic diameter and strong interactions between fluid streams flowing along chevron furrows, accompanied by generation of secondary swirl flows are believed to be the reason for the high heat transfer coefficients.

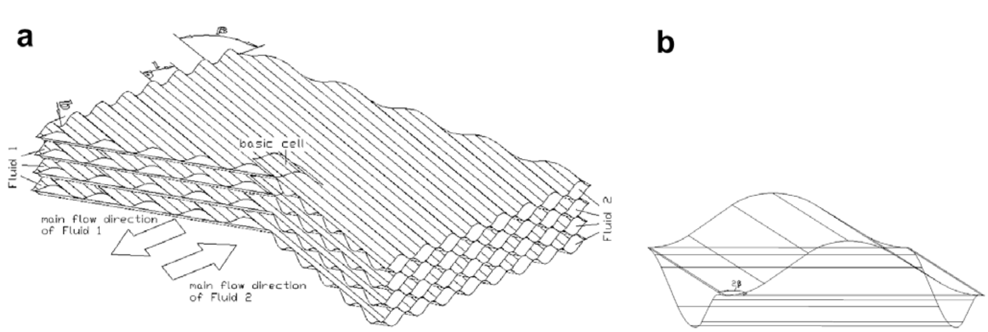

Fig. 1. (a) A cross section of the package of identical corrugated chevron plates. Every second plate is turned 180° thereby forming the complex channels (b) Basic cell consisting of two half ducts, each with sinusoidal cross section.

Results from the performed visualization tests in two corrugated chevron channels with $\beta = 28°$ and $\beta = 61°$ indicate the existence of basically two flow components – the longitudinal, moving in a helix flow pattern in the main direction of the flow and the furrow component, following the direction of the corrugation. Figs. 2 and 3 show the visualization of both components in the channels of different angles β at different *Re* numbers, when the dye was introduced at different locations of the channels' flow cross sections. The flow patterns were recorded at low *Re* number conditions ($Re = 0.1$–250) as they allowed for a clear identification of the flow components. During the tests with plate $\beta = 61°$ the dye was completely diluted starting already at $Re \geqslant 23$–50 (Fig. 3) due to high degree of mixing between components. The furrow flow pattern in the channel with $\beta = 28°$ remained clearly visible at *Re* numbers as high as $Re = 250$, indicating laminar flow. The existence of the flow components is expected also at the fully turbulent flow conditions, which can be seen from the results of numerical simulations of the flow ($Re = 10$–6000) in tested channels [22].

As schematically shown on Fig. 4 the longitudinal component occupies the central part of the flow cross section, changing direction in each cell, passing from one plate to the opposite exhibiting a complex 3D movement. The furrow component flows along the corrugations changing direction only at the plate edges. The relative influence of the two components determines whether the flow pattern is considered as wavy longitudinal or as furrow flow. In general, flow in channels with $\beta > 60°$ will be predominantly wavy longitudinal, while in channels with $\beta < 45°$ the furrow flow pattern prevails. Beside the chevron angle, considered as the most influencing parameter, other parameters like the aspect ratio b/l and flow velocity were shown in the experiments of Price and Fattah [8] and Gaiser and Kottke [14] as well as in the present visualization tests to have significant impact on the relative importance of each flow component. This in turn affects the thermal–hydraulic performances of PHEs, as shown in the experiments of Gaiser and Kottke [15] who tested plates with different b/l at fixed *Re*. It has been found that higher flow velocities (*Re* number), higher aspect ratio b/l (deeper corrugations) and lower chevron angle β will promote furrow flow, which entails reduction of the longitudinal component, and vice versa. Furthermore, an increase of *Re*, β (up to 80°) and b/l will result in better heat transfer and higher pressure drop.

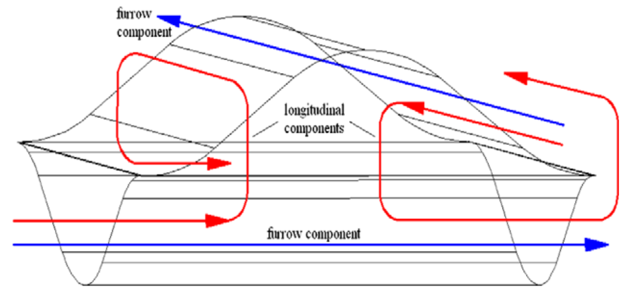

Fig. 4. Principal flow of the two components through the basic cell.

Figs. 2–4 suggest that the furrow component flows in the furrow valleys of successive cells, while the longitudinal component is primarily in a contact with the channel wall in the areas around the furrow crests and cell corners.

Both components and their boundary layers are expected to be disrupted to some extent by mixing between parts of components which are in a contact. That is, however, beneficial for heat transfer. According to the test results from Focke et al. [2], Gaiser and Kottke [15] and Heggs et al. [23], a stronger mixing can be expected at higher β, higher *Re* and lower b/l (shallower corrugations-larger contact area between fluid components). Also, higher β and b/l mean higher effective flow length of both components as well as larger wetted surface area per unit of projected channel

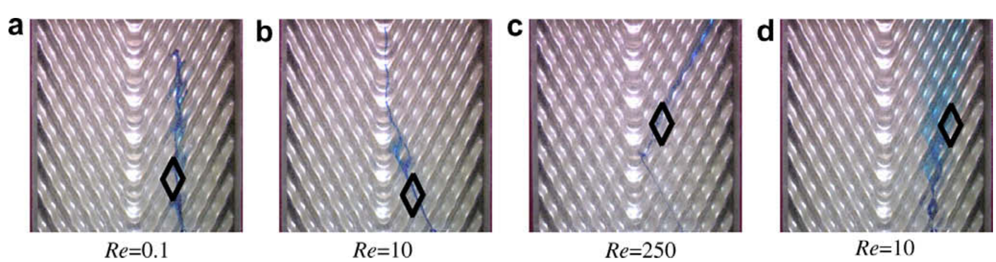

Fig. 2. Flow visualization in the channel with $\beta = 28°$ at different *Re* numbers, (contour of the basic cell is indicated in a bold line). (a) Dye injected close to the transparent wall, test fluid is aqueous glycerol (62% by weight), at very low *Re* number the longitudinal component prevails over most of the cell cross sectional area; (b, c) Dye injected close to the transparent wall, test fluid is water, an increase of the furrow component with *Re* number – typical furrow flow pattern at $Re = 250$. (d) Dye injected in the central part of the flow cross sectional area, test fluid is aqueous glycerol (62% by weight), evidence of the presence of the longitudinal component in the central part of the cell at $Re = 10$ and partial mixing of the flow components.

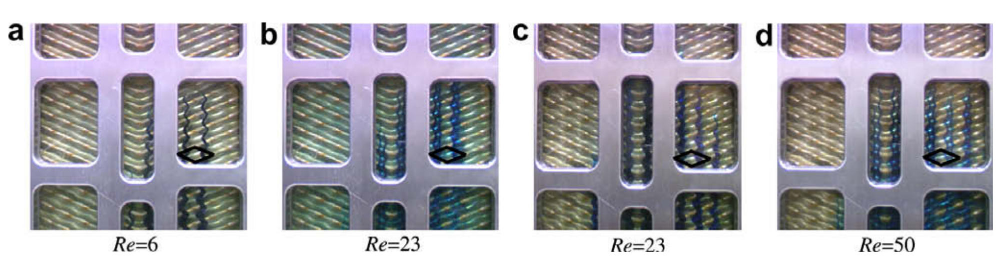

Fig. 3. Flow visualization in the channel with $\beta = 61°$ at different *Re* numbers, (contour of the basic cell is indicated in a bold line). (a, b) Dye injected in the central part of the cross section area, typical wavy longitudinal flow aqueous glycerol (62% by weight), at $Re = 6$ and $Re = 23$, increase of the furrow component with *Re* number and more thorough mixing of the two components within the cell at $Re = 23$. (c, d) Dye injected in the central part of the cross section area, typical wavy longitudinal flow of water at $Re = 23$ and $Re = 50$, different flow pattern at $Re = 23$ compared to the flow with glycerol at $Re = 23$, similar increase of the furrow component (flow pattern) at $Re = 50$ as in the flow of glycerol at $Re = 23$.

surface area, which all entail better thermal performances of PHE channels, but also higher pressure drop.

Recorded flow patterns from Fig. 3 imply presence of likely different flow patterns (different dye dispersion at $Re = 23$) at the same Re numbers when using fluids of remarkably different viscosity i.e. of different velocities at same Re. This indicates possible influence of the velocity of each component as an additional parameter, beside the Re and Pr number solely, on the heat and momentum transfer.

Hence, the heat transfer and pressure drop in corrugated channels of PHEs are influenced by many factors and a mathematical model to describe this complex flow should basically account for:

(1) events within the boundary layers of two flow components; (2) effective flow velocity in corrugations (sine duct); (3) effects of boundary layers disruption and mixing of two flow components; (4) dependence of the effective flow length on the angle β and aspect ratio b/l for both flow components.

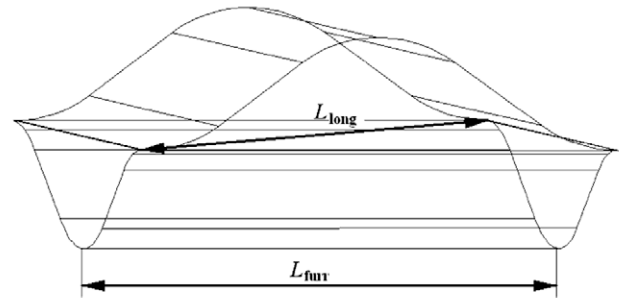

Fig. 5. Definition of the characteristic lengths of the two flow components.

3. Heat transfer and pressure drop in the cell

Heat transfer and pressure drop in the basic cell can possibly be evaluated by means of the analytical solutions derived for sine ducts which are available in the heat transfer literature. The previously mentioned mixing of the flow components and disruption of the boundary layers, could be expected to result in an enhancement of heat transfer and increase of pressure drop compared to a straight duct with sinusoidal cross section. This might all be accounted for by introducing empirically determined correction factors. A selection of a suitable analytical solution is related to the understanding of the flow components behaviour throughout the cell.

After entering the cell, part of the fluid (longitudinal component) is expected to change direction due to interaction with the incoming fluid flowing along the opposite furrow. Consequent change in the velocity profile in turn affects the remaining part of the fluid (the furrow component). Although the mean velocity remains the same, the velocity profiles of both components are thus believed to change throughout the cell, which can also be seen from the results of numerical simulation of flow in PHE channels performed by the present authors in a separate study [22]. Lower velocities are then expected in the central part of the cell [22]. Accordingly, in some part of each cell the flow is expected to possess characteristics of hydrodynamically developing flow. Whether the flow will become fully developed or not is dependent upon the cell dimensions (b/l) and Re number. However, considering the whole channel, a certain variable velocity profile (which varies within each cell in a uniform manner) will already be established after few cells downstream from the entrance [2,23], so that the flow in the channel can in general be regarded as fully developed.

According to Shah [24] laminar flow in sine ducts becomes hydrodynamically fully developed at dimensionless axial distances $x^+ > 0.04$–0.06, depending on the sine geometry (b/l) (see Eq. (6)). No information about the hydrodynamic entrance lengths for turbulent flow in sine ducts have been found in the literature. The same applies for the thermally developing laminar and turbulent flow in sine ducts. For the sine duct geometry of tested channels with $b/l = 0.26$, the dimensionless hydrodynamic entrance length corresponds to $x^+ = 0.053$ [24] i.e. flow will be developed when $x/D_{h,sine} > 0.053 \cdot Re$ where $x = L_{furr}$ (Fig. 5). Since for $b/l = 0.26$ and the range of angles $\beta = (28$–$65)^\circ$ the cell sine duct length to diameter ratio is $L_{furr}/D_{h,sine} = 4.2$–$5.5$ the flow would become hydrodynamically fully developed in the cell sine duct only when $Re < 80$–104. In absence of the data for thermally and simultaneously developing flow in sine ducts, a comparison with corresponding entrance lengths for a circular tube may help in estimating these quantities for sine ducts. The hydrodynamic entrance length in a circular tube calculated by Eq. (1) [25] at fixed diameter is somewhat longer than in a sine duct, e.g. at $Re > 80$–104 for circular tube $L_h/D_h > 4.6$–6, respectively.

$$\frac{L_h}{D_h} = \frac{0.6}{0.035Re + 1} + 0.056Re \tag{1}$$

At the same time, under the simultaneously developing conditions, the thermal entrance length ($L_t/D_h = 0{,}037 \cdot RePr$ for T-boundary conditions [25]) is always longer than the hydrodynamic one for the flow conditions corresponding to those prevailing in present tests i.e. at $Re > 80$–104 $L_t/D_h > 14.8$–19.3 for $Pr = 5$ and $L_t/D_h > 148$–192 for $Pr = 50$. According to this, the laminar flow would always be thermally developing at $Re > 80$–104. Regarding the turbulent flow, the hydrodynamic entrance length in circular ducts is $L_h/D_h > 9.4$ at $Re > 2300$ [26]. The thermal entrance length in turbulent flow is always longer than 10–15 diameters [27] ($L_t/D_h > 10$–15). Following this analysis, the flow within the whole sinusoidal cell might be considered as both hydrodynamically and thermally developing at most of laminar and transient (except at $Re < 80$–104) and all turbulent flow conditions. Indeed, the foregoing analysis is based on the solutions derived for undisturbed flow in the entrance regions of straight circular or sine ducts of constant flow cross section area. For these reasons, it can only give a rough picture what would happen with flow in a cell if the same boundary conditions were applied as for circular or sine ducts, and there were no interactions between flow components. Yet, solutions for the entrance length region could be to some extent applied here as they describe heat transfer and pressure drop in a flow with variable velocity and temperature profiles in the main flow direction, which is most likely the case in sine cells of PHEs.

Accordingly, the energy losses in the entrance and fully developed region of a duct, which occur due to wall shear stress and change in momentum, can be conveniently evaluated by means of the apparent pressure drop factor defined by Eq. (4) [25]. This information about the pressure drop can be simply related to the heat transfer by the generalized Lévêque equation (Eq. (18)), which is well known equation for evaluation of heat transfer in the thermally developing laminar flow. Martin [19] showed that this equation can be successfully employed for heat transfer calculation in PHEs, for laminar but also for turbulent flow, explaining this by the fact that the heat transfer coefficient in the Lévêque equation for a given fluid depends mainly on the product fRe^2 i.e. on the pressure drop which is directly proportional to the fRe^2. Such essential dependence of heat transfer coefficient in PHEs on the pressure drop had already been noticed through experiments in both laminar and turbulent flow regimes [19].

In the present model, each half of the analyzed basic cell is considered as a separate sine duct. This allows application of analytical solutions for the heat transfer and pressure drop in sine ducts, as presented in the following section. The fact there is actually no wall in the central plane of the basic cell is here compensated for by the empirically determined correction factors employed in the Lévêque solution which account for real events in the cell (mixing, swirling, etc.).

4. Mathematical model

4.1. Characteristic length of the flow components

As already mentioned, the furrow component, whose size depends upon the ratio between the two components (i.e. angle β, b/l, Re), passes throughout the cell along valleys occupying certain part of the flow cross section of each cell's half. Then, a characteristic length of such a "micro duct" can be taken as the distance between two crossing points in the furrow direction (see Fig. 5).

Applying the cosinus theorem, the characteristic length for the furrow component is related to the furrow wave length l according to Eq. (2).

$$L_{\mathrm{furr}} = \frac{l}{\sin(2\beta)} \tag{2}$$

Mathematical definition of the longitudinal component's path is a more complex issue as this component follows a 3D path from one half of the cell to the other, changing at the same time direction by the angle 2β. The resultant path is of a helix form. Simplifying this, the characteristic length can be taken as the distance between two crossings in a straight direction of the main flow through the channel, which is also the principal flow direction of the longitudinal component throughout the cell (see Fig. 5). Then, the effective flow length for the longitudinal component equals the pitch and is related to the wave length l according to Eq. (3).

$$L_{\mathrm{long}} = p = \frac{l}{\sin\beta} \tag{3}$$

The true length of the helix 3D path of the longitudinal component is expected to be somewhat higher than L_{long} although it is not passing the longest distance (L_{long}) between the opposite corners of the cell which is a sort of compensation for replacement of the helix path length with L_{long}. Such longer real path allows the longitudinal component to reach the developed flow conditions also at somewhat higher Re numbers than those estimated in the previous section (Re = 80–104) based on a straight flow through sine duct (L_{furr}).

4.2. Friction factor and Nu number calculation

In order to obtain the total pressure drop in the entrance region of a sine duct it is necessary to account for the effects of the wall shear stress and the rate of change in momentum due to the variation of the velocity profile along a duct. Here is used a most convenient approach [25] for practical calculations, whereby the apparent friction factor (referring to the total pressure drop) is divided in two components – one referring to the fully developed flow over the whole duct length (represented by the first term on the right hand side of Eq. (4)) and another one based on the additional pressure drop due to the momentum change and accumulated increment in the wall shear between developing and developed flow (second term on the right hand side of Eq. (4)).

Then, the apparent friction factor for the hydrodynamic entrance region and fully developed flow can be calculated from

$$f_{\mathrm{app}}Re_{\mathrm{sine}} = f_{\mathrm{fully}}Re_{\mathrm{sine}} + K(\infty)/4x^{+} \tag{4}$$

Unfortunately, the incremental pressure drop number which would be calculated for the arbitrary distance x^+ from the sine duct entrance have not been found in the available literature, but only values of $K(\infty)$ calculated for the fully developed region i.e. at the very end of the entrance region [24]. In the present model, $K(\infty)$ is used in Eq. (4) for obtaining friction factor in cases involving both the entrance region and fully developed part as well as for the entrance region only. According to the previous analysis in Section 2 such approach is entirely correct only at lower Re numbers (Re < 80–104) when the hydrodynamic entrance length is believed to be shorter than the length of the cell. Fortunately, at higher Re number when the entrance region possibly extends over the whole cell length, a difference between friction factors obtained with $K(x^+)$ for developing and $K(\infty)$ for developing and fully developed region should be relatively low (<4%) as indicated by the results of calculations performed for the circular duct of same length as the basic cell of tested channels.

The incremental pressure drop number $K(\infty)$ is calculated by Eq. (5) [24].

$$K(\infty) = 2[K_{\mathrm{e}}(\infty) - K_{\mathrm{d}}(\infty)] \tag{5}$$

The dimensionless axial distance is defined as

$$x^{+} = \frac{L_{\mathrm{cell}}}{d_{\mathrm{h,sine}}Re_{\mathrm{sine}}} \tag{6}$$

The effective cell flow length L_{cell} is computed based on the dominant flow pattern:

$L_{\mathrm{cell}} = L_{\mathrm{furr}}$ when $\beta \leqslant 60°$ (the furrow type of flow)
$L_{\mathrm{cell}} = L_{\mathrm{long}}$ when $\beta > 60°$ (the wavy longitudinal type of flow)

Shah [24] presented computed values of $f_{\mathrm{app}}Re$, kinetic energy correction factor $K_{\mathrm{e}}(\infty)$ and the momentum flux correction factor $K_{\mathrm{d}}(\infty)$ in the form of tables as a function of twice the sine duct amplitude to the wave length ratio i.e. the aspect ratio b/l. Based on these tables we have derived, computationally expedient, polynomial functions which can be used instead within the range of $0 < b/l < 0.75$ (Eqs. (7)–(9)).

$$f_{\mathrm{fully}}Re_{\mathrm{sine}} = 2{,}6624x^4 - 10{,}586x^3 + 11{,}262x^2 - 0{,}1036x + 9{,}6 \tag{7}$$

$$K_{\mathrm{e}}(\infty) = -5{,}888x^4 + 9{,}4613x^3 - 4{,}248x^2 - 0{,}1333x + 2{,}648 \tag{8}$$

$$K_{\mathrm{d}}(\infty) = -1{,}7237x^4 + 2{,}7669x^3 - 1{,}2651x^2 - 0{,}0097x + 1{,}512 \tag{9}$$

where the independent variable x is

$$x = \frac{b}{l} \tag{10}$$

The hydraulic diameter of a sine duct, i.e. either half of the cell, is related to the aspect ratio b/l according to Eq. (11) (derived from the data available in Shah [24]).

$$\frac{d_{\mathrm{h,sine}}}{l} = 0{,}1429x^3 - 0{,}6235x^2 + 1{,}0871x - 0{,}0014 \tag{11}$$

Preliminary calculations of a turbulent flow pressure drop throughout the cell's sine duct performed using Filonenko's empirical equation [28], which was originally derived for the developed turbulent flow in a circular duct, resulted in a very low friction factor f_{sine} relative to the experimentally obtained values. Eq. (4) applied for the turbulent flow yielded higher and more realistic values $f_{\mathrm{sine}} = f_{\mathrm{app}}$ as shown later, even though the term $f_{\mathrm{fully}}Re_{\mathrm{sine}}$ in Eq. (4) (constant for a given geometry) is much lower than the product $f_{\mathrm{sine}}Re_{\mathrm{sine}}$ obtained with the mentioned Filonenko's equation. Obviously, the higher values of f_{app} obtained by Eq. (4) are due to dominating influence of the term $K(\infty)/4x^+$, which increases with Re number. This would indicate that a large fraction of energy losses in turbulent flow through the cell occur due to change in momentum rate.

The Re number for one half of the cell is defined by Eq. (12)

$$Re_{\mathrm{sine}} = \frac{u_{\mathrm{sine}}d_{\mathrm{h,sine}}}{\nu} \tag{12}$$

where the average velocity in the cell's sine duct (in the furrow direction) is calculated as

$$u_{\text{sine}} = \frac{\dot{m}_{\text{ch}}}{\rho A_{\text{c,sine}}} \tag{13}$$

and the total channel cross section transverse to the furrow is

$$A_{c,\text{sine}} = bW\cos\beta \tag{14}$$

In the literature, the average velocity u in the channel is often calculated as

$$u = \frac{\dot{m}_{\text{ch}}}{\rho A_{\text{c}}} \tag{15}$$

where the chevron channel cross sectional area transverse to the main flow direction is

$$A_c = bW \tag{16}$$

Re_{sine} and Re number referred to the whole chevron channel (as normally found in the literature) are correlated according to

$$\frac{Re_{\text{sine}}}{Re} = \frac{u_{\text{sine}}}{u}\frac{d_{\text{h,sine}}}{d_{\text{h}}} = \frac{1}{\cos\beta}\frac{d_{\text{h,sine}}}{d_{\text{h}}} \tag{17}$$

The Nusselt number for cell's sine duct is calculated from the Lévêque solution (Eq. (18)) for the thermal entrance region and isothermal (T) boundary condition [25]

$$Nu_{\text{sine}} = 0.40377\left(4f_{\text{app}}Re_{\text{sine}}{}^{2}\text{Pr}d_{\text{h,sine}}/L_{\text{cell}}\right)^{1/3} \tag{18}$$

Nu number referred to the whole cell i.e. channel and Nu_{sine} are correlated by Eq. (19).

$$\frac{Nu}{Nu_{\text{sine}}} = \frac{d_{\text{h}}}{d_{\text{h,sine}}} \tag{19}$$

The friction factor computed for one half of the cell f_{sine} has to be recalculated to obtain the friction factor f defined in the manner as normally done in the literature, where the effective flow length is taken as the overall channel (projected) length and velocity referred to the cross section A_{c}. This friction factor f can also be defined considering only a single cell, as shown in Eq. (20), when the flow length reduces to the cell width in the main flow direction i.e. to L_{long}.

The friction factor f_{sine} (Eqs. (4) and (21)) calculated for the flow throughout cell's sine duct is referred to either $L_{\text{cell}} = L_{\text{furr}}$ or $L_{\text{cell}} = L_{\text{long}}$ depending on the prevailing flow pattern. Two friction factors are then defined and correlated by Eq. (22)

$$f = \frac{\Delta p_{\text{cell}}}{4\left(\frac{L_{\text{long}}}{d_{\text{h}}}\right)\frac{\rho u^2}{2}} \tag{20}$$

$$f_{\text{sine}} = f_{\text{app}} = \frac{\Delta p_{\text{sine}}}{4\left(\frac{L_{\text{cell}}}{d_{\text{h,sine}}}\right)\frac{\rho u_{\text{sine}}^2}{2}} \tag{21}$$

$$\frac{f}{f_{\text{sine}}} = \frac{\Delta p_{\text{cell}}}{\Delta p_{\text{sine}}}\frac{L_{\text{cell}}}{L_{long}}\frac{d_{\text{h}}}{d_{\text{h,sine}}}\left(\frac{u_{\text{sine}}}{u}\right)^2 \tag{22}$$

where $L_{\text{cell}} = L_{\text{furr}}$ when $\beta \leqslant 60^\circ$ and $L_{\text{cell}} = L_{\text{long}}$ when $\beta > 60^\circ$.

As discussed earlier, pressure drop losses along the flat wall in a sine duct can be compensated for in a real cell (in which the central plane wall does no exist) by the losses arising from the interactions between the flow components. Then, if the overall pressure drop Δp_{cell} of fluid streams in the cell is assumed to be equal to the pressure drop in the sine duct Δp_{sine}, the following expressions (Eqs. (23) and (24)) for the channel friction factor f apply

$$\frac{f}{f_{\text{sine}}} = \frac{1}{2\cos^3\beta}\frac{d_{\text{h}}}{d_{\text{h,sine}}} \quad \text{for } \beta \leq 60^\circ \tag{23}$$

$$\frac{f}{f_{\text{sine}}} = \frac{1}{\cos^2\beta}\frac{d_{\text{h}}}{d_{\text{h,sine}}} \quad \text{for } \beta > 60^\circ \tag{24}$$

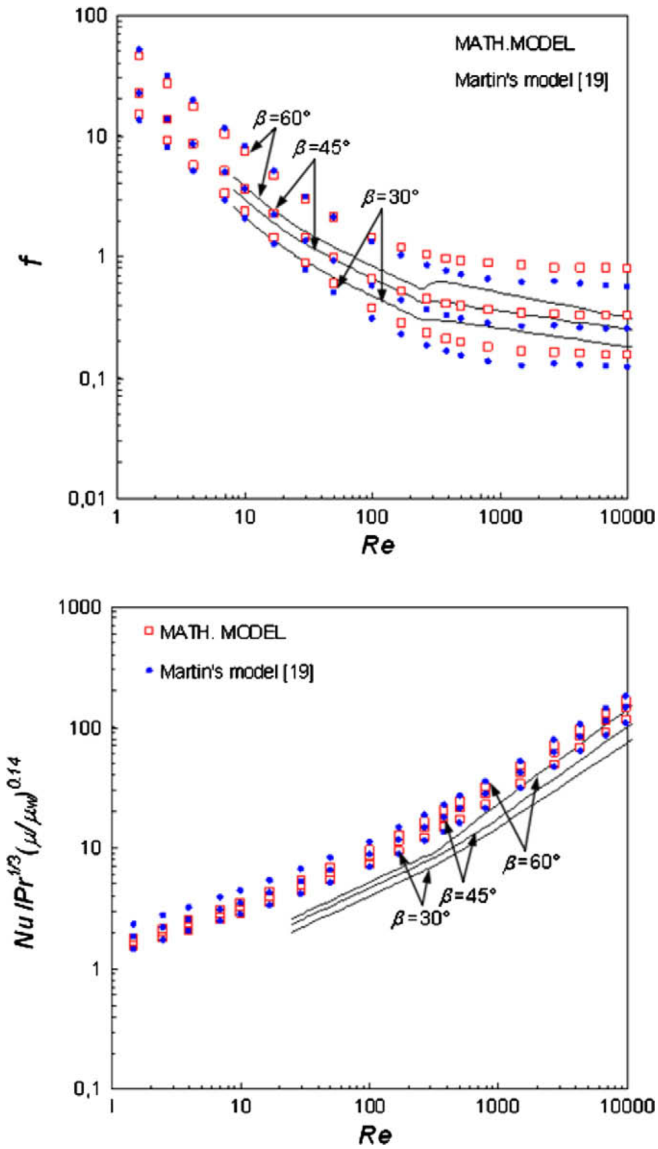

Fig. 6. Comparison of results from the present mathematical and Martin's model [19] with the experiments from Muley et al. [4,5] without applying correction factors on the Lévêque solution in both models.

4.3. Preliminary results from the mathematical model

The diagrams in Fig. 6 show calculated values of f and $Nu/Pr^{1/3}$ obtained by applying the presented mathematical model to the channel geometry used in the experiments of Muley et al. [4,5] whose results are also shown in the diagrams. For comparison, included are also f and $Nu/Pr^{1/3}$ obtained by Martin's model [19], using the same ("uncorrected") constant and exponent in the Lévêque solution as in the present mathematical model (Eq. (18)). Martin [19] based his model on the superposition of two flow components over the range of chevron angles of $\beta = (15–85)^\circ$. Unlike in the present model, the friction factor in Martin's model [19] is directly calculated for the whole channel using standard expressions for the developed laminar and turbulent flow originally developed for a circular tube (for the furrow component) as well as the numerically obtained data for the developed laminar and turbulent flow in the corrugated channel with $\beta = 90^\circ$ (for the longitudinal component). A number of empirically obtained correction factors are then introduced to account for the energy losses due to the flow reversals at the plate edges, crossings between components and change of flow path with the chevron angle. In this way obtained friction factor is then used in the generalized Lévêque solution to calculate Nu number.

Notice that the two different approaches – Martin's [19] and the present one, give similar results for $Nu/Pr^{1/3}$ in absence of empirically determined correction factors. Fairly good agreement between the two sets of calculated friction factors is achieved at $Re < 100$, while at larger Re numbers the present mathematical model yields higher values than Martin's model [19]. In both models change in the inclination of f and $Nu/Pr^{1/3}$ curves occur at $Re \cong 300$ indicating intensification of the heat transfer and pressure drop at higher Re numbers. The same change of the inclination can be observed in the experimental curves of Muley et al. [4,5] at approximately same Re number, Fig. 6.

4.4. Adjustment of the model for heat transfer to experiments

As can be seen from the preliminary results in Fig. 6, the "uncorrected" Lévêque equation (Eq. (18)) proved to be inaccurate in prediction of heat transfer in PHE channels. Therefore, a correction of the constant 0.40337 and exponent 1/3 in Eq. (18) is needed to fit the experimental data i.e. to account for the influence of:

swirling, boundary layer disruption, real effective flow length, separation of flow behind lee crest

These corrections are based on the tests performed by the present authors on channels with $\beta = 28°$ and $\beta = 65°$ as well as on the experimental data of authors who provided the exact geometric data for tested plates (Muley et al. [4,5], Okada et al. [6]). For the best fit, the constant 0.40337 in the Lévêque equation (Eq. (18)) is multiplied by the correction factor 0.38, while the exponent value of 1/3 is replaced with the value 0.375.

After accounting also for a temperature dependent fluid property variation, the deducted semi-analytical equation for heat transfer in PHE channels takes the following form

$$Nu_{\text{sine}} = 0.38 \times 0.40377\left(4 f_{\text{app}} Re_{\text{sine}}^2 d_{\text{h,sine}}/L_{\text{cell}}\right)^{0.375} Pr^{1/3} (\mu/\mu_w)^{0.14} \quad (25)$$

For a given channel geometry (β, b and l), considering Eqs. (2)–(11), the apparent friction factor can be expressed in a generalized form as

$$f_{\text{app}} = \frac{C}{Re_{sine}} + B \quad (26)$$

Then Eq. (25) takes the following generalized form

$$Nu_{\text{sine}} = C_1 \times (C + Re_{\text{sine}} B)^{0.375} Re_{\text{sine}}^{0.375} Pr^{1/3} (\mu/\mu_w)^{0.14} \quad (27)$$

The constants C_1, C and B are functions of the channel geometry and can be directly determined from

$$C_1 = 0.25804 (d_{\text{h,sine}}/L_{\text{cell}})^{0.375} \quad (28)$$

$$C = f_{\text{fully}} Re_{\text{sine}} \quad (\text{calc. by Eq. (7)}) \quad (29)$$

$$B = \frac{K(\infty) d_{\text{h,sine}}}{4 L_{\text{cell}}} \quad (30)$$

e.g. for the tested channel with $\beta = 65°$ and $b/l = 0.26$ the constants are $C_1 = 0.1453$, $C = 10.15$, $B = 0.108$.

Finally, Nu and f referred to the whole channel can be obtained from Eq. (19), and Eqs. (23), (24), respectively.

5. Comparison of the model with experiments

The diagrams in Figs. 7–11 show values of f and $Nu/Pr^{1/3}$ computed by the proposed mathematical model together with the corresponding experimental data available from the open literature and present tests, as well as with the results obtained by Martin's

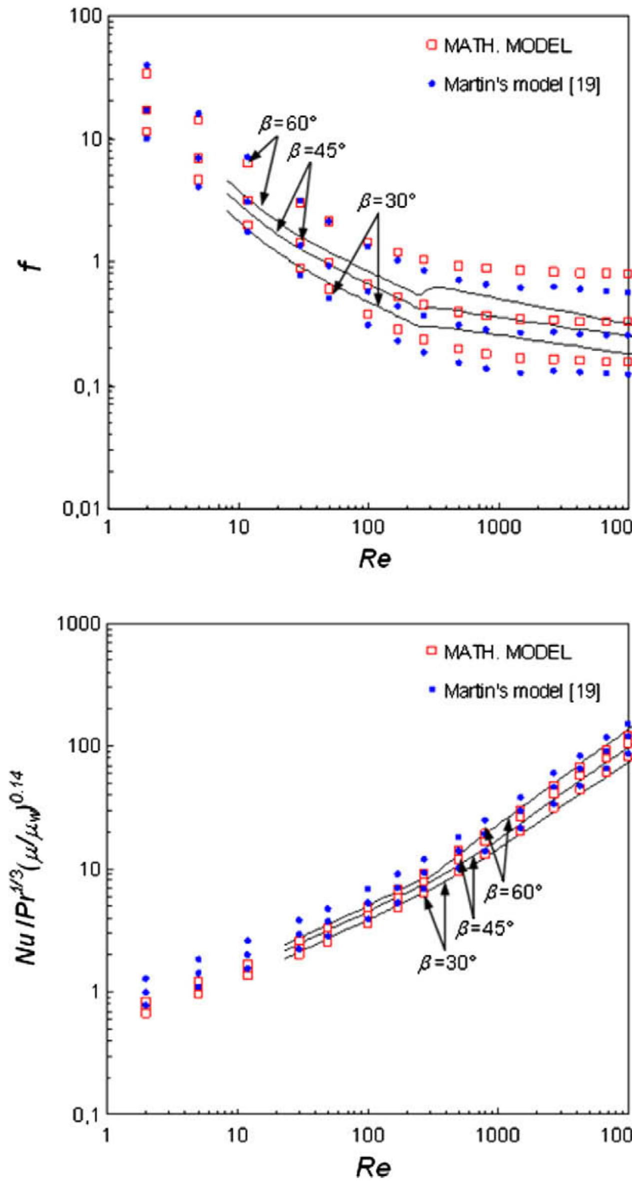

Fig. 7. Comparison between calculated values and the experiments from Muley et al. [4,5].

model [19] (with introduced corrections on the constant and exponent in the Lévêque equation) for a given channel geometry and working conditions. Friction factors from the present tests (Fig. 11) are calculated based on the overall measured pressure drop reduced for the estimated pressure drop in inlet/outlet ports and manifolds (max. 0.5% of the overall) as originally proposed in Shah [20] and later applied in Muley et al. [4,5]. Experimental data of some authors Heavner et al. [3], Muley et al. [4,5], Okada et al. [6] are here recalculated to match the unique way of defining Re number, Nu number and f as used in the present work. In the reviewed literature, only few authors – Muley et al. [4,5], Okada et al. [6] (tests done on scaled up channels) and Focke et al. [2] (mass transfer technique employed on scaled up channels to obtain f and Nu) provided geometrical parameters of tested plates other than the angle β. In other cases presented here (Bond [1], Heavner et al. [3], Thonon et al. [11]), in calculations were used the average values of the most frequently encountered geometric parameters in practice – $b/l = 0.28$ in the case of Thonon et al. [11] and the partially provided parameters (b/p with no reference

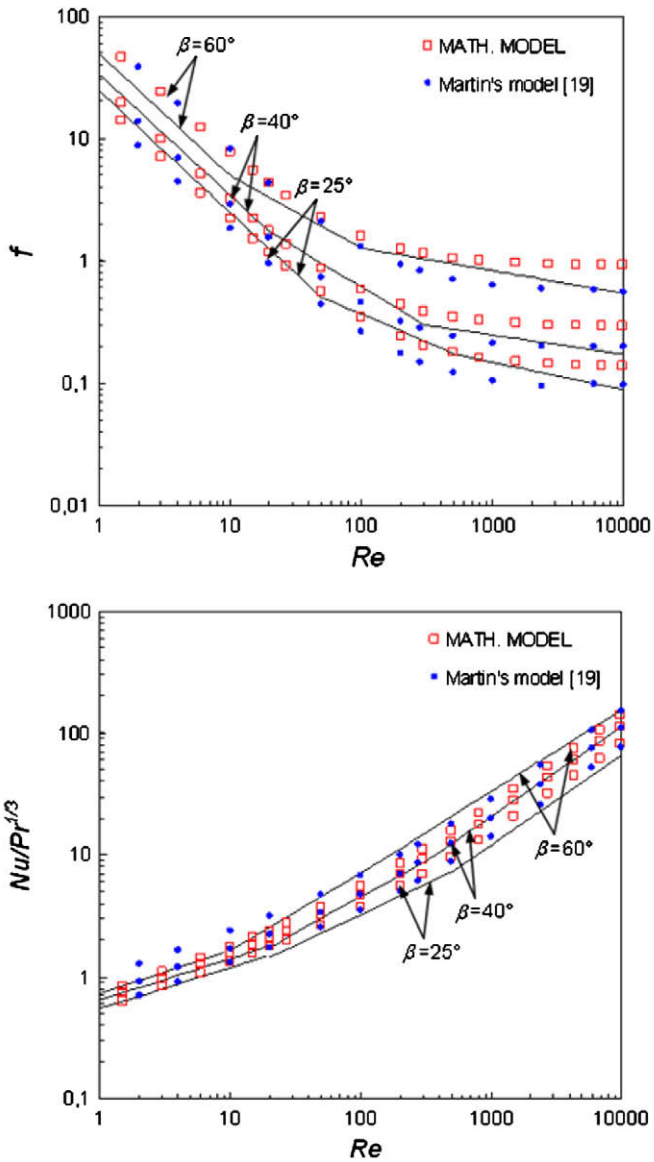

Fig. 8. Comparison between calculated values and the experiments from Bond [1].

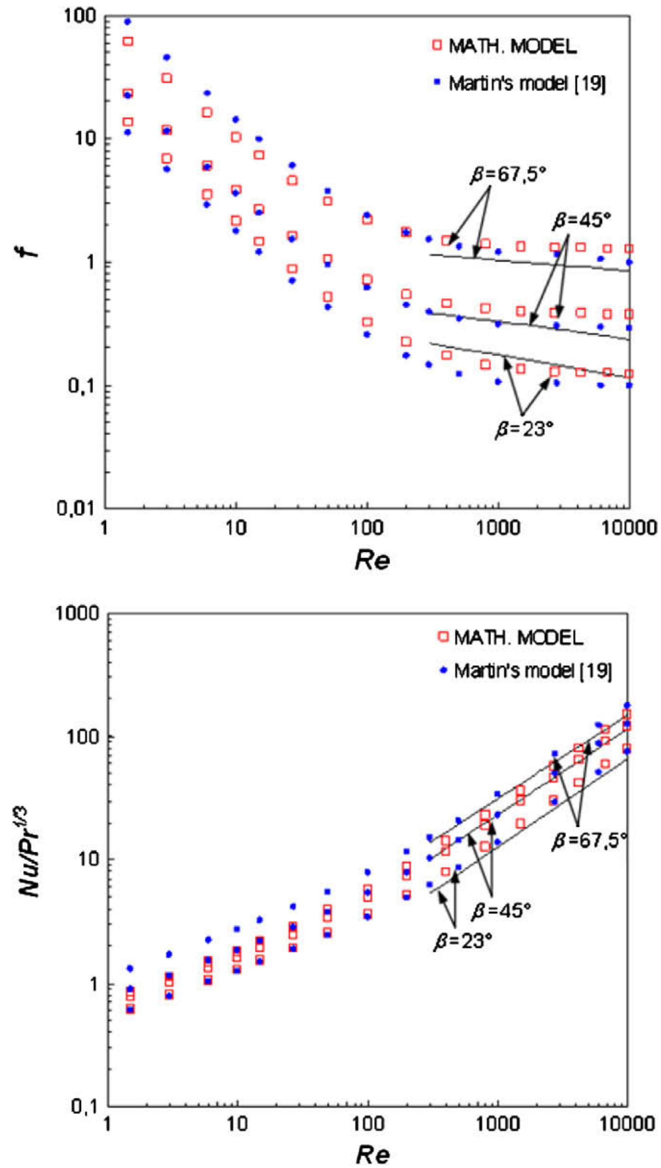

Fig. 9. Comparison between calculated values and the experiments from Heavner et al. [3].

to β) from Bond [1] to which results Heavner et al. [3] have compared their measurements. Geometric parameters of the tested plates compared with the model predictions are listed in Table 1. Since the ratio b/l and d_h influence to some extent calculated values of f_{sine} and Nu_{sine} as well as the recalculation on the channel values, performed comparison is to give a more qualitative picture of the model response on a variation of the angle and flow regime. As can be seen from Table 2, these results are in agreement within ±30% with the present and Martin's model [19] when comparing $Nu/Pr^{1/3}$ and ±(20–60)% for f. The evaluated thermal characteristics by the present model differ up to ±15% relative to the experimental data from Muley et al. [4,5] and ±(20–40)% relative to those from Okada et al. [6]. Discrepancies for the friction factor are larger, in average ±50%. Comparison of Martin's model [19] with the authors who provided exact geometric parameters showed in average larger deviations of computed Nu from the experimental data (up to 35% with Muley et al. [4,5] and up to 30% with Okada at al. [6]). Friction factor obtained by Martin's model [19] deviates from the results of Muley et al. [4,5] up to ±85%.

Diagrams on Fig. 11 provide results from the thermal and hydraulic tests performed by present authors on the two model exchangers with $\beta = 28°$ and $\beta = 65°$, each consisting of three channels (cold fluid in the central channel). The tests were performed with the fluids of distinctively different Pr numbers (water, mixture glycerol/water of 62% and 85% by weight). Values of $Nu/Pr^{1/3}(\mu/\mu_w)^{0.14}$ obtained by the mathematical model agree relatively well (−18% to 7%) with the experimental data at $Re > 50$ (av. deviations for $\beta = 65°$ are as low as ±5%). Larger deviations are present in the very low Re number region at $Re < 10$, especially for the channel 65° (up to 50%) due to sudden deterioration of thermal performance starting at $Re \sim 30$. This has not been previously observed among the thermal experimental data presented in the literature, which are mostly provided for $Re > 10$. Martin's model [19] overestimates the experimental Nu number more than the present model (4–25% at $Re > 50$), which is also specially pronounced at $Re < 10$. Values of f obtained from the present mathematical model are up to 20% higher than the experimental ones at $Re < 50$ and up to 40% higher at $Re > 50$ for the channel with $\beta = 28°$, while larger discrepancies occur for $\beta = 65°$ (up to 50%) at all flow conditions.

Values of f calculated by Martin's model [19] are also in a good agreement (10%) with the experiments for $\beta = 28°$ at $Re < 50$. Larger

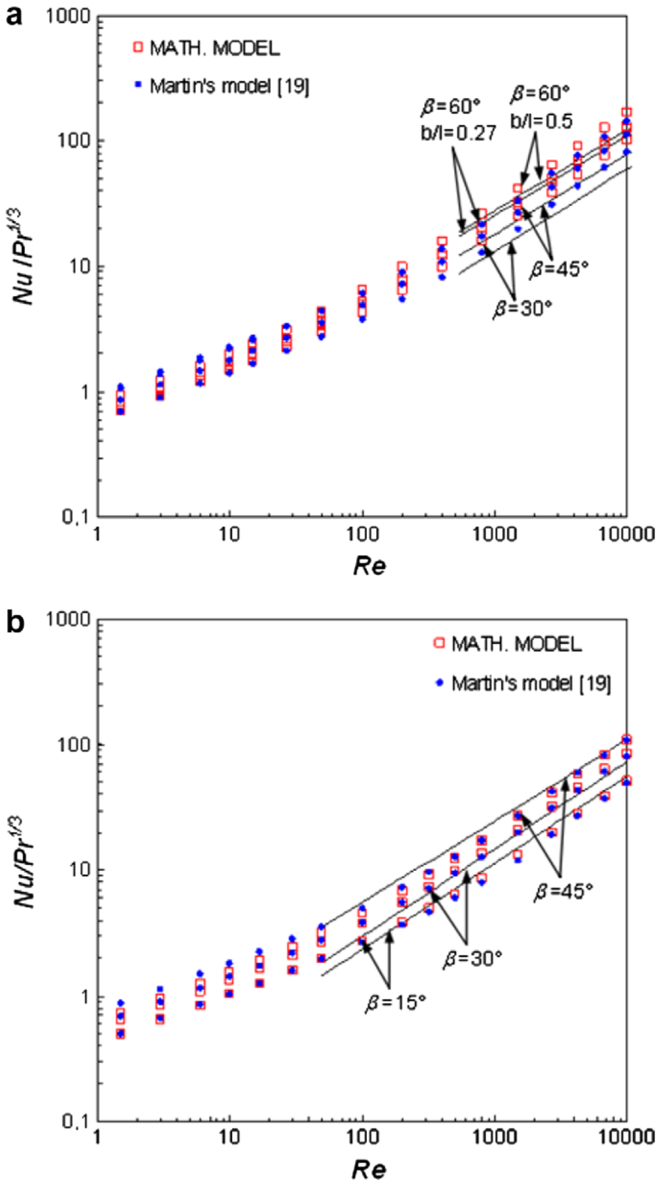

Fig. 10. Comparison between calculated values and the experiments from (a) Okada et al. [6] and (b) Thonon et al. [11].

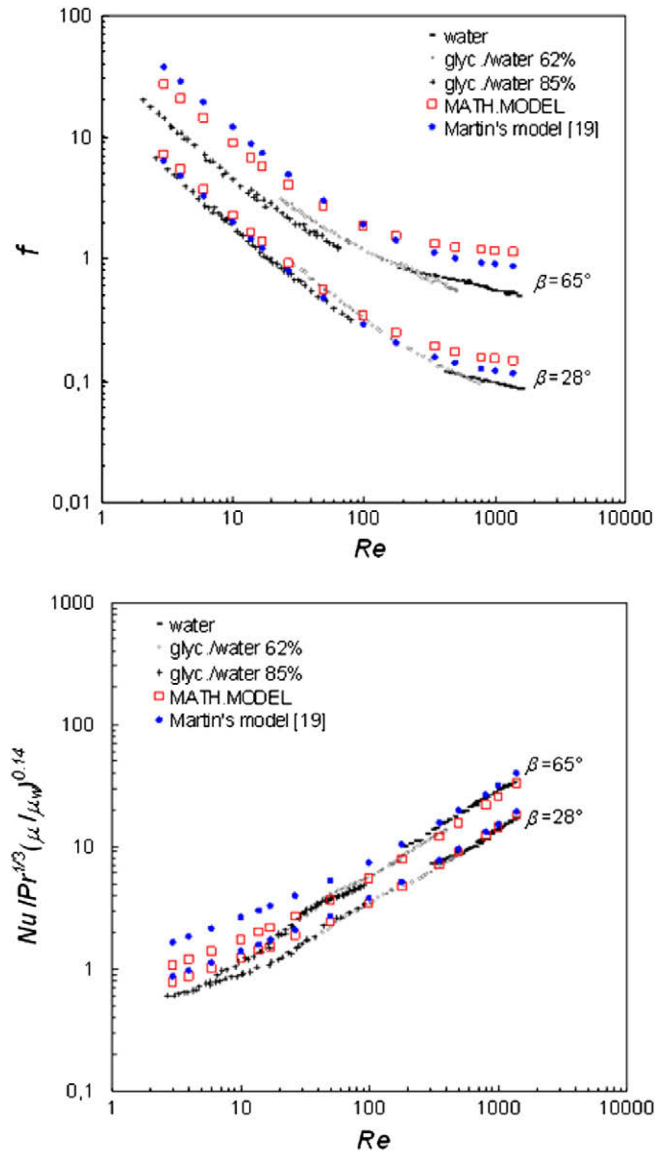

Fig. 11. Comparison between calculated values and the present test values performed with water and glycerol/water mixtures.

deviations are present at $Re > 50$ for both channels-up to 40%, while even larger deviations are observed at $Re < 50$ for $\beta = 65°$ (up to 65%). The slopes of all calculated curves are in good agreement with the slopes of test curves at $Re > 10$.

Influence of the fluid velocity on the flow characteristics is evident from the presence of a clear shift between f curves obtained with different test fluids as well as different slopes of the f curves at $Re = (200–500)$ for $\beta = 65°$ and $Re = (500–770)$ for $\beta = 28°$. At the same Re numbers, when velocities differ by about 10 times, values of f for different fluids differ mutually up to 25% while those of $Nu/Pr^{1/3}\ (\mu/\mu_w)^{0.14}$ up to 15%. The overall measurement uncertainties (including also that in determining the fluid properties) in f and $Nu/Pr^{1/3}\ (\mu/\mu_w)^{0.14}$ are (2.7–4.4)% and (3.6–13.2)%, respectively (the smallest in tests with water and the highest with glycerol/water 85%), i.e. lower than the mentioned shifts between the corresponding curves. Since the thermal and hydraulic characteristic of PHE channels are determined by the size and distribution of flow components in the cell, here presented results would indicate that fluids with different velocities at same Re number do not produce entirely identical flow patterns, as already seen in Fig. 3 at $Re = (23–50)$. All this calls for redefinition of Re number or definition of some other dimensionless quantity which would better reflect present flow conditions.

6. Conclusions

Generalized correlations for prediction of laminar, transient and turbulent flow heat transfer and pressure drop in PHE chevron channels of arbitrary geometry are presented within the corresponding physically based mathematical model. The presented model is based on the observations from the visualization tests of the flow through PHE channels with $\beta = 28°$ and $\beta = 65°$ at $Re = 0.1–250$. Accordingly, the flow characteristics are evaluated by the analytical solutions for the entrance and fully developed region of a sine duct which are then adapted to the basic cell (smallest repeating unit of the channel). Values of $Nu/Pr^{1/3}\ (\mu/\mu_w)^{0.14}$ computed by the presented semi-analytical correlation which was derived from the Lévêque equation, agree in average within ±13% with the data recorded through the measurements performed on

Table 1
Geometric parameters of chevron plates used in the experiments which are compared with the model predictions.

	β, °	b/l	d_h, mm	ϕ
Bond [1]	25, 40, 60	0.35 Estimated[a]	3.2 Estimated[a]	1.26 Estimated[a]
Heavner et al. [3]	23, 45/90 (av.67.5), 45	Estimated[b] 0.35	Estimated[b] 3.2	Estimated[b] 1.26
Muley et al. [4,5]	30, 30/60 (av.45), 60	0.28	3.94	1.21
Okada et al. [6]	30, 45, 60	0.27 (β = 60°) 0.4 (β = 30°,45°) 0.5 (β = 60°)	7 (b/l = 0.27) 6.2 (b/l = 0.4) 5.7 (b/l = 0.5)	1.15 (b/l = 0,27) 1.29 (b/l = 0.4) 1.41 (b/l = 0.5)
Thonon et al. [11]	15, 30, 45	Estim. from typical values 0.28	Estim. from typical values 3.41	Estim. from typical values 1.21
Present experiments	28, 65	0.26	3.45	1.19

[a] Assumption is made that the pressing depth to pitch ratio (b/p = 0.25) Bond [1] provided refers to the β = 45° which yields b/l = 0.35 Eq. (3). ϕ is calculated as a function of b/l using the approximating formula from Martin [19] and d_h is then estimated based on average values of b encountered in a practice (2 mm).
[b] Estimation is based on the plate geometry of Bond [1] as Heavner et al. [3] have not reported the plates geometric parameters and have compared their data only with the results from Bond [1].

Table 2
Deviations of $Nu/Pr^{1/3}$ and f calculated by the present and Martin's model [19] from the experimental data.

		Present math. model		Martin's model [19]	
		$Nu/Pr^{1/3}$	f	$Nu/Pr^{1/3}$	f
Bond [1]	Mean deviation, % Deviation interval (95.5% data)	−2.0 −30 to 26	10.0 −18 to 38	6.0 −19 to 31	−6.0 −49 to 37
Heavner et al. [3]	Mean deviation, % Deviation interval (95.5% data)	−1.0 −18 to 16	11.0 −18 to 40	7.4 0 to 15	−20.0 −65 to 25
Muley et al. [4,5]	Mean deviation, % Deviation interval (95.5% data)	−0.5 −16 to 15	4.0 −47 to 55	16.5 −3 to 36	9.7 −91 to 110
Okada et al. [6]	Mean deviation, % Deviation interval (95.5% data)	9.3 −24 to 43		12.5 −8 to 33	
Thonon et al. [11]	Mean deviation, % Deviation interval (95.5% data)	0.4 −29 to 30		3.5 −26 to 33	
Present experiments $Re \geqslant 50$	Mean deviation, % Deviation interval (95.5% data)	−4.8 −18 to 7	38.5 5 to 53	10.5 4 to 25	 3 to 41
Present experiments $Re < 50$	Mean deviation, % Deviation interval (95.5% data)	20.5 −10 to 51	23.3 −6 to 52	37.5 7 to 68	21.5 −22 to 65

the channels with β = 28° and β = 65° at Re = 50–1400; within ±15% with the experimental data of Muley et al. [4,5] at Re = 10–10,000 and in average within ±35% with the data from Okada et al. [6]. In all other cases, where the geometrical parameters of tested plates were not completely provided, the discrepancies between computed and experimental thermal data lie within ±30%. As a comparison, the results from another generalized equation for $Nu/Pr^{1/3}$ $(\mu/\mu_w)^{0.14}$ provided in Martin [19] agree with the present experimental data within 25% at Re > 50, from the data of Muley et al. [4,5] within 35% and data from Okada et al. [6] in average within 30)%. Performed experiments revealed sudden decrease of Nu number at Re < 30 for plate with β = 65°. Since f still remains significantly higher than in the channel with β = 28°, this would favour use of plates with lower angles for very low Re number applications.

Relatively larger disagreement ±(10–50)% between the experimental values of friction factors and those obtained by the adapted, but basically analytical solution for a sine duct is expected, since no empirical correction factors are employed (due to large discrepancies within the experimental data), as succeeded for Nu number. These factors should otherwise account for the pressure losses due to interactions of the flow components and change of the direction in a cell. Nevertheless, the computed values are in line with the experiments over the wide range of Re numbers, which would indicate that most of the pressure losses occur due to momentum change i.e. due to variable velocity profile in the cells. This assumption is further supported by the fact that the solutions for fully developed flow available in the literature yield much lower pressure drop than is experimentally determined.

Presented experiments, which were performed with different viscosity fluids (such as water and glycol/water mixture), showed that different flow velocities may produce different flow patterns at the same Re numbers which finally results in different values of Nu and f at fixed Re numbers. This would call for redefinition of Re number and/or introduction of some other dimensionless quantity in presentation of the thermal–hydraulic characteristics, which would better reflect actual flow pattern.

Provided solutions for prediction of heat transfer and pressure drop in PHE channels have been shown to give results which are consistent with the experiments for a wide range of flow conditions and geometrical parameters β and b/l. They can be useful in situations when no experimental data are available for particular flow regime and geometry, as well as at a designing stage for optimizing plate geometry to particular working conditions. Further refinement of the suggested expressions is recommended through a comparison with more experimental data for plates of various geometries.

Acknowledgments

This research was carried out at the Department of Energy Technology, Royal Institute of Technology, Stockholm, Sweden and supported by SWEP International AB, Sweden.

References

[1] M.P. Bond, Plate heat exchangers for effective heat transfer, Chem. Eng. 367 (1981) 162–166.
[2] W.W. Focke, J. Zacharadies, I. Olivier, The effect of the corrugation inclination angle on the thermohydraulic performance of plate heat exchangers, Int. J. Heat Mass Transfer 28 (1985) 1469–1479.
[3] R.L. Heavner, H. Kumar, A.S. Wanniarachchi, Performance of an industrial plate heat exchanger: effect of chevron angle, AIChE Symp. Ser. 89 (1993) 262–267.
[4] A. Muley, R.M. Manglik, Experimental study of turbulent flow heat transfer and pressure drop in a plate heat exchanger with chevron plates, ASME J. Heat Transfer 121 (1999) 110–117.
[5] A. Muley, R.M. Manglik, H.M. Metwally, Enhanced heat transfer characteristics of viscous liquid flows in a chevron plate heat exchanger, ASME J. Heat Transfer 121 (1999) 1011–1017.
[6] K. Okada, M. Ono, T. Tomimura, T. Okuma, H. Konno, S. Ohtani, Design and heat transfer characteristics of new plate heat exchanger, Heat Transfer Jpn. Res. 1 (1972) 90–95.
[7] A.F. Savostin, A.M. Tikhonov, Investigation of the characteristics of the plate heating surfaces, Therm. Eng. 17 (1970) 75–78.
[8] A.F. Price, A.-F.M.-A. Fattah, Hydrodynamic characteristics of a plate heat exchanger channel, Trans. Inst. Chem. Eng. 56 (1978) 217–228.
[9] A.C. Talik, L.S. Fletcher, N.K. Anand, L.W. Swanson, Heat transfer and pressure drop characteristics of a plate heat exchanger using a propylene-glycol/water mixture as the working fluid, in: Proc. 1995 Nat. Heat Transfer Conf., ASME, New York, vol. 12, 1995, pp. 83–88.
[10] A.C. Talik, L.W. Swanson, L.S. Fletcher, N.K. Anand, Heat transfer and pressure drop characteristics of a plate heat exchanger, in: Proc. ASME/JSME Therm. Eng. Conf., Maoui, Hawaii, vol. 4, 1995, pp. 321–328.
[11] B. Thonon, R. Vidil, C. Marvillet, Recent research and developments in plate heat exchangers, J. Enhanced Heat Transfer 2 (1995) 149–155.
[12] L.L. Tovazhnyanski, P.A. Kapustenko, V. Tsibulnik, Heat transfer and hydraulic resistance in channel of plate heat exchangers, Energetika 9 (1980) 123–125.
[13] W.W. Focke, P.G. Knibbe, Flow visualization in parallel-plate ducts with corrugated walls, J. Fluid Mech. 165 (1986) 73–77.
[14] G. Gaiser, V. Kottke, Effects of corrugation parameters on local and integral heat transfer in plate heat exchangers and regenerators, in: Proc. 9th Int. Heat Transfer Conf., Jerusalem, Israel, vol. 5, 1990, pp. 85–90.
[15] G. Gaiser, V. Kottke, Effects of wavelength and inclination angle on the homogeneity of local heat transfer coefficients in plate heat exchangers, in: Proc. 11th Int. Heat Transfer Conf., Heat Transfer 1998, Kyongju, Korea, vol. 6, 1998, pp. 203–208.
[16] L.E. Haseler, V.V. Wadekar, R.H. Clarke, Flow distribution in a plate and frame heat exchanger, in: Proc. 1st European Conf. on Therm. Sci., IChemE Symposium Series, vol. 1, no. 129, 1992, pp. 361–367.
[17] G. Rosenblad, A. Kullendorff, Estimating heat transfer rates from mass transfer studies on plate heat exchanger surfaces, Wärme-und Stoffübertragung 8 (1975) 187–191.
[18] A.S. Wanniarachchi, U. Ratnam, B.E. Tilton, K. Dutta-Roy, Approximate correlations for chevron-type plate heat exchangers, in: Proc. 1995 Nat. Heat Transfer Conf., ASME, New York, vol. 12, 1995, pp. 145–151.
[19] H. Martin, Theoretical approach to predict the performance of chevron-type plate heat exchangers, Chem. Eng. Process 35 (1996) 301–310.
[20] R.K. Shah, W.W. Focke, Plate heat exchangers and their design theory, in: R.K. Shah et al. (Eds.), Heat Transfer Equipment Design, Hemisphere Publ., New York, 1988, pp. 227–254.
[21] D. Dović, The analysis of single-phase flow in chevron channels of plate heat exchangers, Int. MSc Thesis, Energy Department, Royal Institute of Technology, Stockholm, 2000.
[22] D. Dović, S. Švaić, Experimental and numerical study of the flow and heat transfer in plate heat exchanger channels, in: Proc. 10th Int. Refrig. Air Condit. Conf., Purdue, Indiana, 2004, pp. 1–8.
[23] P.J. Heggs, P. Sandham, R.A. Hallam, C. Walton, Local transfer coefficients in corrugated plate heat exchanger channels, Trans. Inst. Chem. Eng. 75 (Part A) (1997) 641–645.
[24] R.K. Shah, Laminar flow friction and forced convection heat transfer in ducts of arbitrary geometry, Int. J. Heat Mass Transfer 18 (1975) 849–862.
[25] R.K. Shah, A.L. London, Laminar Flow Forced Convection in Ducts, Advances in Heat Transfer, Academic Press, New York, 1978. pp. 99–143.
[26] A. Galović, Technical Thermodynamic II, University of Zagreb, Zagreb, 1997. pp. 58–62.
[27] W.M. Kays, M.E. Craford, Convective Heat and Mass Transfer, second ed., McGraw-Hill, New York, 1980. pp. 237–271.
[28] S. Kakac, Y. Yaman, Convective Heat Transfer, CRC Press, Boca Raton, 1995. pp. 292–298.